Post-print version:

Co-Located Wind-Wave Farms: Optimal Control and Grid Integration

H. del-Pozo-Gonzalez, F.D. Bianchi, and J.L. Domínguez-García

This work has been published in **Energy**:

H. del-Pozo-Gonzalez, F.D. Bianchi, and J.L. Domínguez-García, "Co-Located Wind-Wave Farms: Optimal Control and Grid Integration", *Energy*, vol. 272, pp. 127176, 2023.

Final version available at:

URL: https://www.sciencedirect.com/science/article/pii/S0360544223005704

DOI: 10.1016/j.energy.2023.127176

BibTex:

```
@Article{del-Pozo-Gonzalez2022,
    Title   = {Co-Located Wind-Wave Farms:  Optimal Control and Grid Integration},
    Author  = {Hector del-Pozo-Gonzalez, Fernando D. Bianchi, and Jose Luis
       Domínguez-García},
    Journal = {Energy},
    Year    = {2023},
    Number  = {},
    Pages   = {127176},
    Volume  = {272},
    Doi     = {10.1016/j.energy.2023.127176}
}
```

Co-Located Wind-Wave Farms: Optimal Control and Grid Integration

Hector Del Pozo Gonzalez[a], Fernando D. Bianchi[b], Jose Luis Dominguez-Garcia[a], Oriol Gomis-Bellmunt[c]

[a] *Catalonia Institute for Energy Research (IREC), Jardins de les Dones de Negre 1, 2ª. - 08930 Sant Adrià de Besòs, Barcelona, Spain*
[b] *Instituto Tecnológico Buenos Aires (ITBA) and Consejo Nacional de Investigaciones Científicas y Técnicas (CONICET), Iguazú 341, C1437, Ciudad Autónoma de Buenos Aires, Argentina.*
[c] *Centre d'Innovacio Tecnologica en Convertidors Estatics i Accionaments (CITCEA), Departament d'Enginyeria Electrica, Universitat Politecnica de Catalunya (UPC), Barcelona 08028, Spain*

Abstract

Nowadays, offshore renewable energy is seen more and more as an attractive alternative to onshore energy thanks to less space limitations and usually better weather conditions. However, the higher costs in installation and maintenance demand a continuous search for higher conversion efficiency in order to achieve an economically viable electricity generation. In this line, the co-location of wind and wave power sources might serve to reduce the generation power variability and also to take advantage of using the same infrastructure and implementation area. Several studies have been carried out mainly focused on determining possible zones of implantation or developing new co-location concepts. However, the optimization and control of these new offshore energy conversion systems have not been extensively studied in the literature. This article presents a new optimal control strategy for co-located wind and wave farms in order to fulfill the operation and integration requirements demanded by power system operators. The proposed control scheme is evaluated in several realistic scenarios. The obtained results show that with adequate control strategies, it is possible to increase the electricity production of co-located wind-wave farms satisfying the frequency requirements of the network, even in adverse events, and also to increase the total power reserve of the system.

Keywords: Co-located Wind-Wave; Combining Renewable; Offshore Wind Energy; Wave Energy; Power Reserve; Grid Stability.

1. Introduction

The development of offshore renewable energy (wave, tidal and offshore wind energies) has been established as one of the EU's energy objectives for 2050. The target is to reach an installed capacity of 188 GW in wave and tidal energies and 460 GW in offshore wind energy [1]. In this line, the co-located wind-wave farms (WWFs) have arisen as a promising alternative for combining both technologies in order to achieve a more efficient use of the farms' exploitation areas and thus increase the generated power density (W/m^2) [2]. According to [3], the co-locating offshore wind and wave energy farms may allow a smoother power generated output compared to the wind or wave farms operating independently. In [3], it is reported that co-located

*Corresponding author
Email address: hdelpozo@irec.cat (Hector Del Pozo Gonzalez)

WWFs are able to achieve a reduction in the power variability equivalent to those achieved by the aggregate energy of two offshore wind farms separated near 500 km or two wave farms with 800 km of separation.

This is a new topic and therefore the available literature is not extensive. Most of the articles focus on the energy harvesting potential of particular implementation zones [3, 4, 5]. A summary of the different layout configurations of the co-located farms can be found in [1]. Astariz et al. [6] study uniformly distributed arrays and analyze the benefits of the co-location from the point of view of maintenance and operation. Regarding grid integration, Lund [7] studies the effects of combining different generation sources (e.g. solar, wind, and wave) on the electrical grids. The effects on the transmission capacity of co-located WWFs is analyzed in [8]. Several works study the variability of the generated power, for instance, Tedeschi et al. [9] propose the integration of batteries in the co-location of wind and wave farms. Other works are focused on the potential power variability reduction that can be achieved in particular areas [10, 11]. Saenz et al [12] study the role wave energy converters (WECs) to maximize the auxiliary power supply and their optimal combination with offshore hydrogen. A life cycle cost (LCC) analysis is presented by Clark et al. [13] considering the wake effect in WWFs. The results suggest that floating wind-wave co-located arrays are advantageous in terms of LCC compared to WEC-only or floating wind turbine-only arrays. On the other hand, to the best of the author's knowledge, the complete system control of co-located wind-wave plants does not seem to be analyzed in the literature.

Several technologies have been proposed for harvesting energy from waves. Clearly, the most suitable technologies for co-location with monopile or floating wind turbines are those based on floating WEC concepts. These devices are usually made up of a buoy and a Power Take-Off (PTO) system. The latter is the part in which the mechanical power captured from the waves is converted into electricity. A number of control tools have been used in WECs, such as latching, sliding mode or model predictive control (MPC), among others. Latching is based on reducing the phase change between the speed of the buoy and the excitation force by locking the PTO for a period of time [14, 15, 16]. The aim is to operate the device near resonance in order to increase the power absorption. Sliding mode control has been used in [17, 18] to track a velocity reference and thus improve the energy harvesting. MPC have been employed in [19, 20] to maximize the captured energy by optimizing the excitation force. With the aim of saving costs and increasing the power generation, WECs are often gathered in arrays. In [21], Bacelli et al. have found that a coordinated control instead of individual controls for each device might improve the overall energy capture. However, as this approach needs to share information among devices, this also results in less reliable systems.

The control of wind turbines have been extensively analyzed in the literature, see e.g. [22]. The control of wind farms considering the particular wind conditions faced by each turbines is a topic that have arisen considerable interest in the last years. The most common objective is to maximize the energy capture. However, other concepts have been proposed aiming to exploit available degrees of freedom. For example, in [23], the power tracking is combined with the reduction of fatigue damage in order to increase the useful life of the turbines. Other proposals aim to increase the power reserve [24] or provide ancillary services to the

grid [25].

Stability is crucial in power systems and might be affected by the integration of renewable energy sources [26, 27]. In case of integration of WEC farm, Ekström et al. [28] propose the control of a marine substation that connects and disconnects WECs depending on the state of the sea, a strategy that can also be used in case of WWFs. The effects of the aggregation of wave energy on the load flow and system stability is studied in [29]. In case of wind farm integration, in [30, 31, 32], it is presented coordinated strategies for the integration of wind power plants in AC networks to provide frequency support. However, the power system stability involving WWFs has not been analyzed in the literature.

The purpose of this article is to analyze the potential of coordinated controls for co-located WWFs. The main contributions can be summarized as:

- Modelling of WWFs for analyzing the behavior of WECs and wind turbines and evaluating coordinated control strategies.
- A two-level control scheme to coordinate the power contributions of WEC and wind turbines arrays in order to minimize the power fluctuations caused by WECs, to provide frequency support, and to optimize the overall power reserve.

The proposed control scheme is evaluated by simulation in a realistic case of study with three AC areas, two onshore conventional power plants and an offshore WWFs, inspired in possible implantation plans for the PLOCAN (Plataforma Oceánica de Canarias) area [33].

The present paper is organized as follows. Section 2 introduces the co-located wind-wind farms. In Sections 3 and 4, the modelling and control of waves and offshore wind power plants are presented, respectively. Section 5 describes the proposed two-level control strategy aimed to coordinate the power contributions of WECs and wind turbines. Then, simulation results are presented in Section 6. Finally, some conclusions are drawn in Section 7.

2. Co-Located Wind-Wave Farms

2.1. Co-located WWF Layouts

Figure 1 illustrates three possible layouts for co-located WWFs as proposed in [1]. The green area represents the power system to which the WWF is connected. The peripherally distributed array (layout a) in Figure 1) consists in surrounding the wind farm by the WECs, especially on the sides more distant from the shore, in order to capture most of the incident waves and minimize the radiation effects from the farm's wind turbines. In the alternate row array (layout b), rows of WECs are placed between rows of wind turbines. In the case of monopile or spar wind farms, the turbines are usually spaced 3D-5D-7D. The WECs can be located in the intermediate rows as the radiation and diffraction effects are not very noticeable [34]. Finally, in the layout c), the WECs and wind turbines are located in two separate areas and only share the infrastructure to connect them to the land consumes.

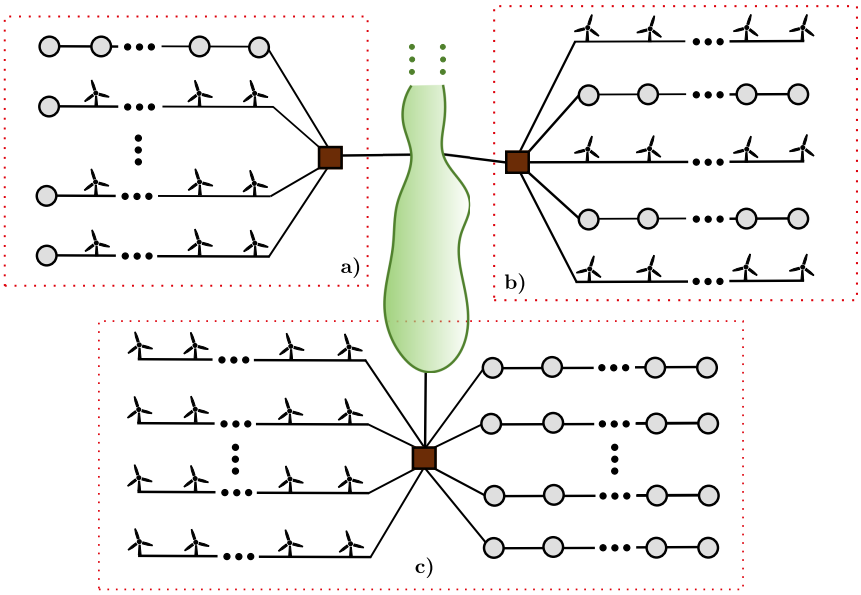

Figure 1: Three possible layouts of co-located wind-wave farms: **a)** peripherally distributed array, **b)** alternated row array and **c)** co-located independent array.

2.2. Grid-connected Wind-Wave Farms

The integration of WWFs into a power system may affect the stability of the entire system due to the high power fluctuations introduced by this type of generation. System stability problems can be local or global and can be caused by different agents (loads, generation, lines, etc.). These can be classified into voltage, generator-rotor-angle or frequency stability problems. As the present work is only focused on active power generation, only the frequency stability problem will be analyzed here. The frequency fluctuations are caused by imbalances between the demanded and generated power. As active power generated by wind and wave farms may exhibit significant fluctuations, a WWF may cause frequency stability problems. In order to reduce this undesirable effects, it is necessary to smooth the power injected into the land grid. A common strategy is to maximize the power produced by the WECs and reduce the power fluctuations injected into the land grid by controlling the power delivered by the wind farm. Therefore, the capability for minimizing frequency errors depends on the system power reserve that can be maintained by the wind farm and the onshore generation.

Figure 2 sketches a three-area electrical network with two onshore generation points and a WWF connected via HVAC submarine cable that will be used to analyzed the proposed control strategy for compensating frequency fluctuations. The WWF is assumed to be an alternate row array. This layout is preferred mainly due to its potential to share wind farm collectors or also the possibility of sharing moorings/anchors. The present study focused on the power production and integration. As a consequence, the spacing between WECs will be assumed larger than 10 radius. In this circumstance, the interaction among WECs can be neglected as the radiation and diffraction effects are not noticeable [21]. The power system consists of two onshore

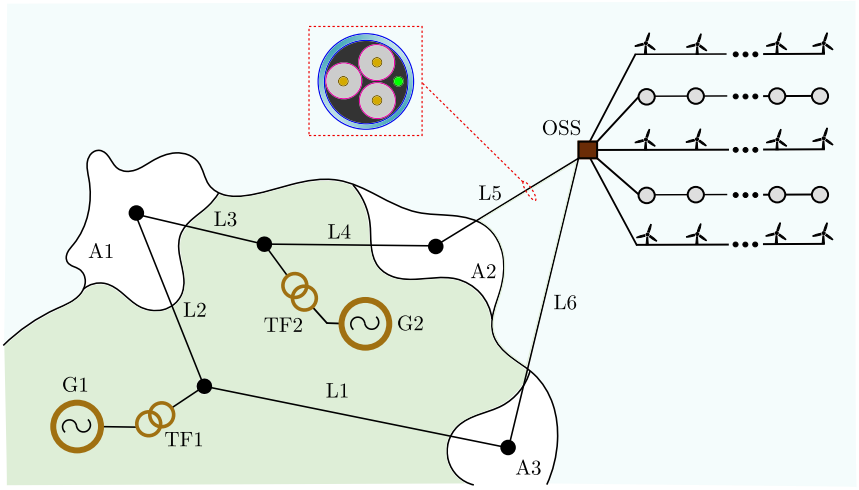

Figure 2: An example of a three-area electrical network with two onshore generation points and a WWF connected via HVAC submarine cable.

generation plants and the co-located WWF. The onshore generation plants are modeled as synchronous generators represented by a fourth-order two-axis model. All the generation plants are interconnected with three AC areas modeled as power loads. Each generator is connected to the lines by the respective transformer. The WWF also includes a transformer in the offshore sub-station (OSS). The WWF is connected through submarine HVAC cables to the respective onshore points. A detailed description of the system will be introduced in Section 6.

The algebraic equations corresponding to the power flow of the system formed by the generation (onshore and WWF), the submarine cables, transformers, lines between areas and the areas' power loads allow us to obtain the following dynamic model of the entire system:

$$\dot{X} = f(X, Y, U), \tag{1}$$

being

$$X = \begin{bmatrix} x_{ps}^T & x_{wwf}^T \end{bmatrix}^T, \tag{2}$$

$$Y = \begin{bmatrix} I_{dq}^T & V^T & \theta^T \end{bmatrix}^T, \tag{3}$$

$$U = \begin{bmatrix} U_1^T & \dots & U_n^T \end{bmatrix}^T. \tag{4}$$

The symbol x_{wwf} denotes the state vector of the co-located WWF formed by the respective wind and wave generation and $x_{ps} = [x_{g,1} \dots x_{g,i}]^T$ the state vector of the power system including the onshore generation, where:

$$x_{g,i} = [\delta_i \ \omega_i \ E'_{q,i} \ E'_{d,i} \ E_{fd,i} \ V_{R,i} \ R_{F,i}]^T \tag{5}$$

represents the state vectors of the i^{th} generator plant ($i = 1, \dots, n$), which as mentioned before are modeled as synchronous generators with a fourth-order two-axis model. Note that the injected active power depends

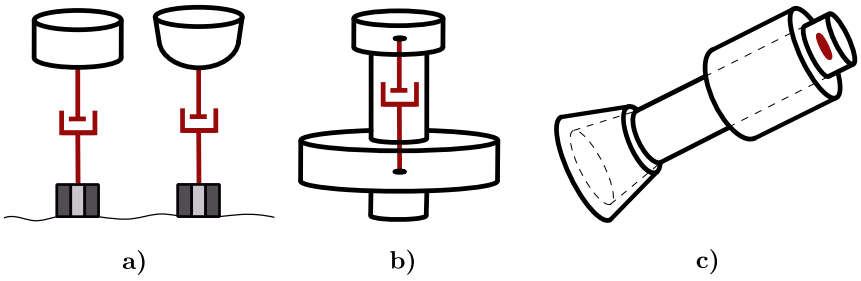

Figure 3: Schematic representations of the most common floating WECs: **a)** point absorbers, **b)** two-body WECs and **c)** spar oscillating water column

on the variables of these generators: $P_i(\delta_i, I_{d,i}, I_{q,i}, V_i, \theta_i)$, being the i^{th} torque angle, d-q currents, voltages and phases, respectively.

The next sections present the wind and wave energy system and the corresponding control in detail.

3. Wave Power Generation

Wave energy systems can be located onshore (on the coast), nearshore and offshore. However, when they are co-located with floating wind farms, only nearshore and offshore result adequate. The devices in these areas can be floating or submerged. In this work, we will focus only on floating devices.

3.1. Floating Wave Energy Converters

Figure 3 illustrates the main floating WEC technologies. Figure 3a depicts the so-called floating point absorbers, which are simple buoys that oscillate with the movement of the waves and generate energy by reacting with the seabed. Its behavior corresponds to a mass-spring-damper and their power generation is proportional to the relative movement in heave (the z-axis). The most common WECs are the floating wave energy converters shown in Figure 3b. These WECs consists of a floating and a submerged part, and the PTO captures the energy through the relative motion between them. This type of technology was initially described in [35] and a control scheme can be found in e.g. [36]. Finally, Figure 3c corresponds to a floating Oscillating Water Column (OWC), more specifically the well-known Spar-Buoy OWC [37, 38]. This device is usually anchored to the seabed, can move freely and is open at the bottom. The PTO is an air turbine. When the OWC hits the waves, the turbine converts the bidirectional induced air flow into electrical power [38]. Owing to the maturity and simplicity of the floating point absorbers [39, 40], this will be the WEC technology considered in the scheme proposed in this article.

3.2. The WEC Model and the Equation of Motion

In case of a heaving point-absorber with a rigid connection with the PTO system, the floater only oscillates up and down. Therefore, its equation of motion can be expressed in terms of the Newton's second law as:

$$M\ddot{z}(t) = F_w + F_{hs} + F_{rad} + u, \tag{6}$$

being F_w the external forces produced by the movement of the waves, F_{hs} the hydrostatic forces of the device, F_{rad} the radiation forces generated by the floating bodies, and u is the control action applied to the PTO. Since the working principle of WECs is based on the wave energy absorption, the radiation effects caused by the own device are the most significant term in the previous equation. That is, the WEC average absorbed power can be expressed as $\bar{P}_{abs} = \bar{P}_w - \bar{P}_{rad}$, being $\bar{P}_w$ the average power of the wave and $\bar{P}_{rad}$ the average radiated power. Based on the Cummins model [41], the radiation force is given by:

$$F_{rad} = -\mathcal{A}_\infty \ddot{z}(t) - \int_0^t L_r(\tau)\dot{z}(t-\tau)\,\mathrm{d}\tau, \tag{7}$$

where $\mathcal{A}_\infty$ is the infinite added mass matrix and L_r the radiation kernel. This kernel can be connected with the damping coefficient $\mathcal{B}_\omega$ using the expression:

$$L_r(t) = \frac{2}{\pi}\int_0^t \mathcal{B}_\omega(\omega)cos(\omega t)\,\mathrm{d}t. \tag{8}$$

The infinite added mass matrix is computed as:

$$\mathcal{A}_\infty = \lim_{\omega\to\infty} A_\omega(\omega), \tag{9}$$

being $A_\omega(\omega)$ the added mass coefficient matrix at a certain frequency ω. Assuming pure sinusoidal signals, the radiation force can be approximated by constant coefficients [20], yielding to:

$$F_{rad} = -\mathcal{A}_\omega \ddot{z}(t) - \mathcal{B}_\omega \dot{z}(t). \tag{10}$$

The hydrostatic force is given by:

$$F_{hs} = \rho g \pi r^2 z(t) = K_{hs,z} z(t), \tag{11}$$

where K_{hs} is the buoyancy stiffness coefficient. Consequently, the Newton's equation (6) can be rewritten as:

$$(M + \mathcal{A}_\omega)\ddot{z}(t) + \mathcal{B}_\omega \dot{z}(t) + K_{hs,z} z(t) = F_w + u, \tag{12}$$

being u the force applied in the PTO. Then, defining $x_1 = z$ and $x_2 = \dot{z}$, the previous equation can be cast as the set of ODEs:

$$\dot{x}_1 = x_2, \tag{13}$$

$$\dot{x}_2 = \frac{1}{m}(F_w - K_{hs,z}x_1 - \mathcal{B}_\omega x_2 + u), \tag{14}$$

where $m = M + \mathcal{A}_\omega$.

3.3. An Optimal Control Strategy for the WEC

The WEC needs a control strategy in order to maximize the energy harvesting. Here, an optimal latching strategy will be used due to its simplicity and good performance. A detailed description of this control can be found in [15, 16]. Basically, an optimal latching consists in reducing the phase change between the speed

of the buoy and the excitation force by locking the PTO during a period of time. The objective is to induce a resonance effect and thus increase the energy capture. To this end, the latching controller aims to cancel the damping term in (14) applying a force:

$$u = -\mathcal{C}_p \gamma x_2, \tag{15}$$

where $\mathcal{C}_p$ is a damping coefficient sufficiently large to stop the device motion and γ is the control action. The control law is a bang-bang strategy, i.e. γ takes two values, 0 or 1. When $\gamma = 0$ the point absorber is free to oscillate, and when $\gamma = 1$ is locked. The algorithm to decide the value of γ at each time step is based on the optimal control theory and aimed to maximize power absorption. Basically, the goal is to find an admissible control signal that maximizes the objective functional:

$$\max_u J(u) = \frac{1}{t_f} \int_0^{t_f} \mathcal{B}_w x_2^2(t,u) dt, \tag{16}$$

corresponding to the energy absorbed from the wave excitation in the time interval $[0\, t_f]$.

In order to solve this optimization problem, the corresponding Hamiltonian is computed as:

$$\begin{aligned} &\mathcal{H}(x, u, \lambda_1, \lambda_2, t) = \\ &= u\, x_2 + \lambda_1 x_2 + \frac{\lambda_2}{m} \left(F_w - \mathcal{B}_\omega x_2 - K_{hs,z} x_1\right) + u, \end{aligned} \tag{17}$$

where $x = [x_1\ x_2]^T$. Hence, its time derivative is

$$\dot{\mathcal{H}} = \frac{\partial \mathcal{H}}{\partial t} + \dot{x}^T \frac{\partial \mathcal{H}}{\partial x} + \dot{u}^T \frac{\partial \mathcal{H}}{\partial u} + \dot{\lambda}^T \frac{\partial \mathcal{H}}{\partial \lambda}, \tag{18}$$

where $\dot{\lambda}^T$ corresponds to the adjoint matrix. By applying the Pontryagin's Maximum Principle along the optimal path that maximizes the Hamiltonian at each time instant:

$$\mathcal{H}(x^*, u^*, \lambda^*, t) \geq \mathcal{H}(x^*, u, \lambda^*, t), \tag{19}$$

with the superscript $*$ meaning the optimal value. Since the Hamiltonian is a linear function of γ, the optimal command can be expressed as:

$$\gamma = \begin{cases} 1, & \text{if } \ \lambda_2 \mathcal{C}_p x_2 < 0, \\ 0, & \text{otherwise}, \end{cases} \tag{20}$$

see [16] for more details.

The operation of the latching control strategy (15) can be observed in the simulation results presented in Figure 4. These results correspond to the ideal point absorber given in [15], with a radius of 5 m and a mass of 1 tonne, subjected to irregular sea states (see Appendix). The top and middle plots in Figure 4 show the position and velocity of the buoy without and with the control law (15). As can be observed, the optimal latching increases the velocity and position compared with the open-loop case. In the middle plot, it is possible to see the successive locking of the WEC during the time the velocity is zero. When unlocked, the velocity presents a steeper increase and a larger amplitude. This increases the energy captured as observed in the bottom plot in Figure 4, in accordance with the minimization of the objective (16).

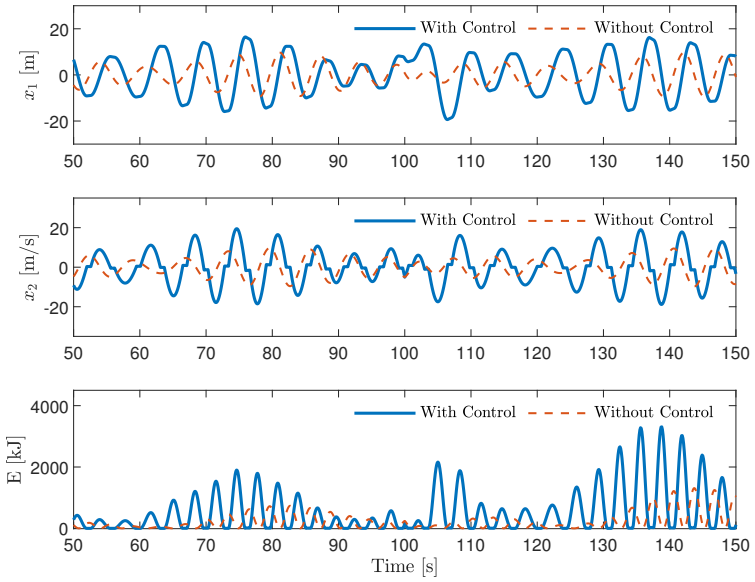

Figure 4: Simulation responses corresponding to an ideal point absorber with a radius of 5 m and a mass of 1 tonne, subjected to irregular sea states with and without control

Taken into account that the WECs do not interacted each other, the total power captured by an array of m devices can be expressed as:

$$P_g^{wave} = \sum_{i=1}^{m} P_m^i, \tag{21}$$

where P_m^i is the power absorbed by each device.

4. Offshore Wind Power Generation

4.1. Wind turbine model

The wind power plant with k turbine is modeled as an equivalent one producing the total power. The dynamics is represented by a two-mass model connected by a gearbox of ratio N_g. The characteristic equations of the system are:

$$J_r\dot{\omega}_r = T_r - B_s\omega_s - K_s\theta_s, \tag{22}$$

$$J_g\dot{\omega}_g = \frac{B_s}{N_g} + \frac{B_s}{N_g}\theta_s - T_g, \tag{23}$$

where ω_r and ω_g are the rotor and generator speeds, respectively. The symbols J, T, K and B refer to inertia, torque, stiffness and damping, respectively, and the subscripts r, s and g denote the rotor, stator and generator, respectively. The relative angle of rotation between the rotor and generator satisfies:

$$\dot{\theta}_s = \omega_r - N_g^{-1}\omega_g \tag{24}$$

Regarding the aerodynamic part, the wind power P_w corresponding to an airflow passing through a rotor surface A_r with an effective wind speed v is given by

$$P_w = \frac{1}{2}\rho_w A_r v^3, \tag{25}$$

being ρ_w the air density. This power can only partially be converted into mechanical power by the turbine. The power fraction is governed by the power coefficient C_p that depends on the blade pitch angle β and the tip-speed-ratio $\lambda = \omega_r R/v$, with R the rotor radius. Therefore, the power generated by the wind turbine is given by

$$P_g = \frac{1}{2}\rho_w A_r C_p(\beta, \lambda) v^3. \tag{26}$$

The torque developed by the turbine is

$$T_r = \frac{1}{2}\rho_w A_r \frac{C_p(\beta, \lambda)}{\omega_r} v^3. \tag{27}$$

The power captured by the turbine can be controlled by modifying the pitch angle β and rotor speed ω_r [22, 42]. The total power generated by the wind farms is assumed given by

$$P_g^{wind} = \sum_{i=1}^{k} P_g^i, \tag{28}$$

where P_g^i is the power produced by each turbine.

4.2. Control and de-loading operation

Each wind turbine is assumed following the de-loading control strategy shown in Figure 5, [43, 32]. The wind farm controller sent a power reference P_{res} to each turbine, which may be lower than the rated power P_{rated}. If the turbine is facing an effective wind speed lower than v_{res}^w, it will deliver the maximum power available. Otherwise, the wind turbine will work in a de-loaded mode keeping a reserve given by $P_{rated} - P_{res}$. Thus, certain amount of power is available to contribute in the frequency regulation or other ancillary services. Here, this reserve will be used to compensate the WEC fluctuations.

5. Overall control strategy for co-located WWFs

Figure 6 shows the proposed control strategy for the co-located WWF integration into a network such as the one presented in Figure 2. The strategy coordinates the contributions of the co-located WWF according to the energy demands of the AC areas and ensures the network stability. This is a centralized control with a two-level structure. The lower level aims to guarantee the stability of the network, mainly in events of frequency and voltage drops caused by the fluctuations in the power generation. Whereas the upper level focuses on managing the available power produced by the WWF and the demands of the local areas. For this purpose, this level produces the power set-points for each generation system while fulfill an optimal power flow.

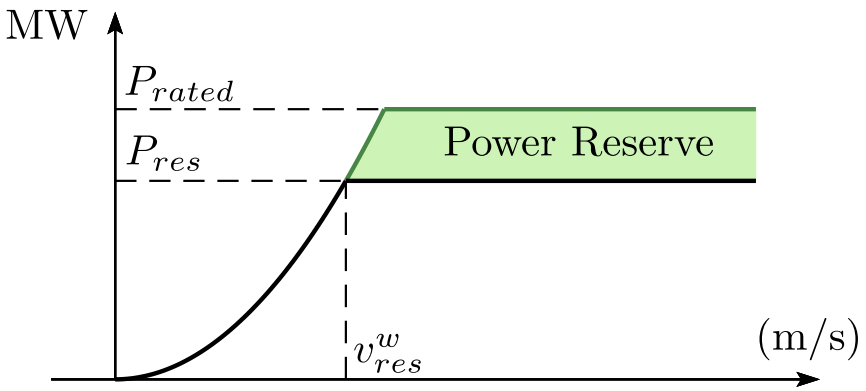

Figure 5: Power-wind speed curve corresponding to a de-loading strategy

5.1. Upper-Level Control Design

In the proposed control strategy, it is assumed that each WEC produces the maximum power, and the wind turbines operate in de-loaded mode. Firstly, it is sought the control action $P_r^{wwf} \in \mathbb{R}$ that ensures the system power balance. This is a set-point that must satisfy the overall WWF and is computed according the following error tracking expression:

$$P_r^{wwf} = P_{ref} - P_{gen}, \tag{29}$$

being:

$$P_{gen} = \sum_{i=1}^{n_g} P_g^{Gi}, \tag{30}$$

$$P_{ref} = \sum_{i=1}^{n_d} P_{dem}^{Ai} \tag{31}$$

where A and G denote the areas and generators, respectively. The total power P_r^{wwf} that must produce the WWF is the sum of the power P_g^{wave} generated by the WECs and the power P_g^{wind} produced by the wind farm.

In order to translate the command P_r^{wwf} into individual commands for each turbine, the upper level control takes into account the information provided by the supervisors of the wind farm and the WEC array. These supervisors manage the communications with each energy conversion devices with the aim of measuring the total available power. That is, the power transmission is shared by both arrays, but not the communications in order to ensure a reliable set-point computation. The wave supervisor computes the value P_g^{wave} according to (21) with the information sent by each WEC in the array. On the other hand, the wind farm supervisor communicates the generated power P_g^{wind} and the available power P_{av}^{wind} to the central control.

In addition, this supervisor produces the power set-points $P_r^{wind} \in \mathbb{R}^k$ for each turbine according to the generation target P_{rt}^{wind} for the entire wind farm sent by the central controller. This reference is computed

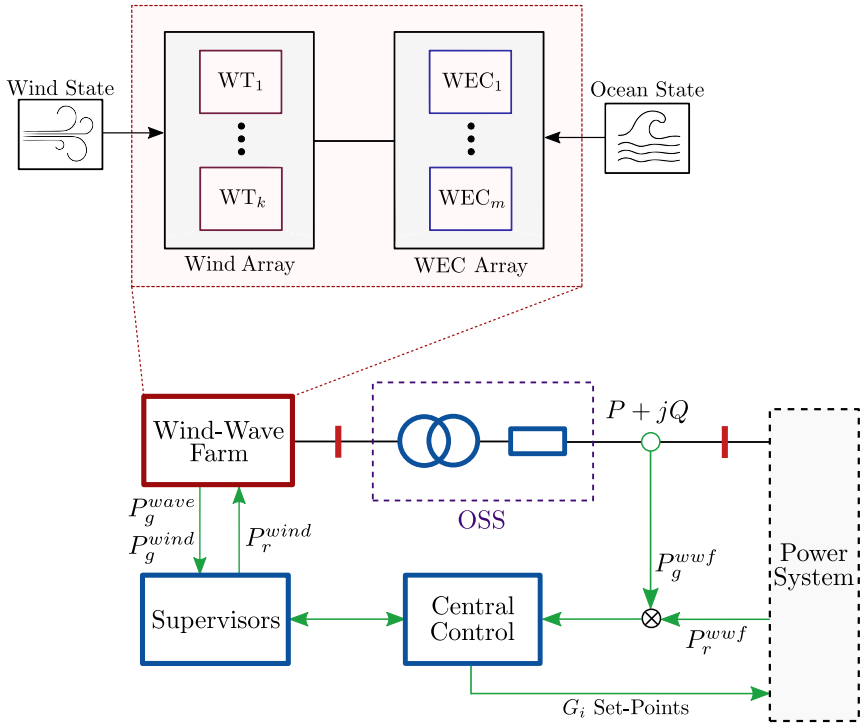

Figure 6: Proposed two-level control scheme for co-located WWFs

as

$$P_{rt}^{wind} = P_r^{wwf} - P_g^{wave}, \tag{32}$$

The reference wind power P_r^{wind} must be within the P_{av}^{wind} limits, defined at each time instant by:

$$P_{av}^{wind} = P_g^{wind} + P_{res}^{wind}, \tag{33}$$

being P_{res}^{wind} the total power reserve in the wind farm. When the wave power P_g^{wave} is sufficient to decrease the wind power P_g^{wind} and thus increases the power reserve, the command computation satisfies the following maximization problem:

$$\begin{aligned} \max_{P_r^{wind} \in \mathbb{R}^k} \quad & P_{res}^{wind} \\ \text{s.t.} \quad & (32) \text{ and } (33) \end{aligned} \tag{34}$$

5.2. Lower-Level Control Design

As a consequence of the high variability of the renewable power sources, especially the one coming from the WEC array, there exist some periods of time in which the power distribution of the upper-level controller is not able to fulfill the power balance (29). For these periods of time, the proposed strategy includes a low-level control that acts on the inland generator set-points in order to minimize the frequency fluctuations caused by the mentioned power mismatch. To this end, the low-level controller produces small adjustments

of the power set-points of the generators, computed to satisfy the following quadratic cost function:

$$J = \frac{1}{2}\int_0^\infty (\mathbf{X}^T\mathbf{Q}\mathbf{X} + \mathbf{U}^T\mathbf{R}\mathbf{U})dt \tag{35}$$

where $\mathbf{X}$, $\mathbf{U}$ are the state variables and inputs of the linearized system (1) and $\mathbf{Q}$ and $\mathbf{R}$ are diagonal weighting matrices penalizing the torque angle, angular frequency and control inputs, respectively. The matrix $\mathbf{Q}$ is determined from the dominant eigenvalues of the closed-loop system [44].

Clearly this low-level control is centralized and communication losses might affect it. However, the communications involved in this control consists only of inland lines, more reliable and less prone to fail than offshore infrastructure.

6. Results

The proposed strategy is evaluated with the case of study illustrated in Figure 2. The power system consists of a steam generation plant (G_1), a diesel generation plant (G_2) and the co-located WWF. The generators are interconnected with three AC areas modeled as constant power loads. Each generator is connected to the lines through transformers and HVAC cables. As mentioned in Section 4, the wind farm in the WWF is modeled as an aggregated wind turbine. The system under study is made up of 14 wind turbines and 74 WECs, whose parameters can be found in Table 4, together with the main parameters of the network. The data for the WECs were adopted from [15], the wind turbines correspond to the NREL 5MW model [42], and the network parameters were adapted from a networked area system described in [26]. As mentioned in Section 2, wake effects and interaction among WECs are neglected due to the spacing between wind turbines and WECs.

The wind and wave profiles corresponds to the North-East coast of Gran Canaria (Spain). Table 1 summarizes the correlation data between wind speed and wave height for this implantation area: the PLOCAN (Plataforma Oceánica de Canarias) area. On the other hand, Table 2 lists the frequency distributions of significant wave height and spectral peak period [33].

In order to evaluate the correct behavior of the controlled system, four scenarios were analyzed. The first three scenarios analyze the short-term operation (timescale of seconds) and the last one the long-term behavior (timescale of hours). The first scenario studies the nominal operation, that is, the wind and wave generation complement each other to satisfy the demand. The second scenario presents a higher absorption of wave energy, which means that the wind power reserve can be increased, as described in the previous sections. Then, due to the control is centralized, the behavior of the system in the event of communications losses is evaluated. The fourth scenario evaluates a long-term operation with the most probable wind-wave conditions for the North-East coast of Gran Canaria (Spain). This conditions are depicted in Table 1, showing wind speed and significant wave height (H_s). The peak period T_p was obtained from the probability correlation shown in Table 2.

H_s	Wind Speed (1-hour at 10m)										
	0 - 2	2 - 4	4 - 6	6 - 8	8 - 10	10 - 12	12 - 14	14 - 16	16 - 18	18 - 20	>20
0.00 - 1.00	2.083	8.396	12.354	8.754	4.174	1.685	0.588	0.144	0.044	0.010	0.001
1.00 - 2.00	3.012	12.063	18.533	12.298	5.582	2.195	0.777	0.248	0.062	0.010	0.006
2.00 - 3.00	0.384	1.387	2.041	1.568	0.785	0.295	0.126	0.055	0.012	0.003	0.002
3.00 - 4.00	0.014	0.060	0.109	0.076	0.034	0.009	0.007	0.003			
4.00 - 5.00			0.005	0.003							

Table 1: Gran Canaria Wind-Wave Data [33]

H_s	Peak Period (T_p)													
	1-2	2-3	3-4	4-5	5-6	6-7	7-8	8-9	9-10	10-11	11-12	12-13	13-14	14-15
0.00 - 1.00	0.037	0.771	2.603	4.524	5.392	4.907	4.211	3.504	2.836	2.252	1.766	1.244	0.827	0.512
1.00 - 2.00	0.001	0.3	1.845	5.132	10.973	14.608	9.569	5.006	3.119	1.865	1.250	0.823	0.542	0.326
2.00 - 3.00				0.003	0.049	0.465	2.593	2.552	1.087	0.522	0.275	0.161	0.12	0.085
3.00 - 4.00							0.012	0.11	0.147	0.073	0.028	0.005	0.001	0.002
4.00 - 5.00									0.001	0.003				

Table 2: Gran Canaria Significant Wave Height - Peak Period Probability [33]

6.1. Scenario 1: Nominal operation

Figure 7 shows simulation results corresponding to nominal operation under calm sea. In the top plot can be observed the WWF power demand P_r^{wwf} (purple line), the total power generated by the wind farm P_g^{wind} (blue line), the total power provided by the WEC array P_g^{wave} (red line), and the total power delivered by the WWFs P_r^{wwf} (yellow line). The power demand is around 65 MW and most of power generated by the WWF comes from the wind farm. In this scenario, the power demand is lower than the WWF rated value and the system is capable of satisfying the demand. As the sea is calm, the wave power is rather smooth.

The middle and bottom plots allow us to see the low-level control operation aimed to compensate the small mismatch between the power produced by the WWF and the demand, which may affect the frequency. The middle plot shows, in per unit, the power injected by the two onshore generators, P_{G_1} (blue line) and P_{G_2} (red line), necessary to stabilize the frequency. The bottom plot compares the frequency variation around the nominal value 50 Hz when the low-level control is active (blue line) and is inactive (red line). Clearly, this control is able to significantly prevent the wave power fluctuations from being directly delivered into the grid and thus affect frequency of the entire power system.

6.2. Scenario 2: High wave power absorption

In Figure 8, it can be observed simulations corresponding to higher wave power conditions. The higher average wave power allow us to increase the wind power reserve. Compared to the previous case, in which the wind power generation was close to 60 MW, now it is delivering 50 MW into the grid, that is an increase of 10 MW in the power reserve. On the other hand, the additional increase in the wave power also causes

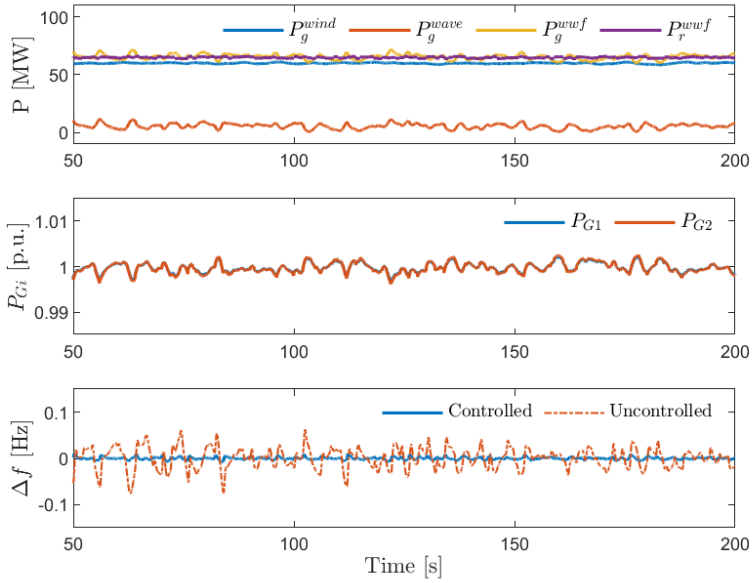

Figure 7: Scenario 1: Nominal operation under calm sea

higher fluctuations in the total power. These fluctuations must be compensated by the low-level control in order to avoid high frequency deviations. The effect of this control can be seen in the middle and bottom plots. Focusing on the bottom one, the blue line is the frequency after applying the low-level control, which is significantly smoother than the uncontrolled value (red line).

6.3. Scenario 3: Communication Faults

Since the control is centralized, the effects of communication failures on the proposed scheme must be analyzed. For this purpose, it is assumed that the onshore communication is robust, but the communications with the offshore plant may fail. In this scenario, the central controller may lose information about the WWF generation, but not about the rest of the power system. That is, the central controller has no information about the power generated by the WWF and cannot send the corresponding set-points. This leads to the incorrect operation of the upper-level control. However, as the power transmission remains unaffected, the onshore local measurements and the information of the rest of the power system allow the proper functioning of the lower-level control.

Figure 9 shows simulation results corresponding to this scenario when communications are lost in the interval between 90 and 160 s. As a consequence, the upper-level controller do not have the current power output information from the WWF and is not able to produce the correct commands. At 90 s, time of communication loss, due to the lack of set-points from the central controller, the local control at each turbine tries to maximize the energy capture. Hence, until the moment in which communications are restored (160 s), the total generation of the WWF is higher that the demanded power. This implies that the power generated

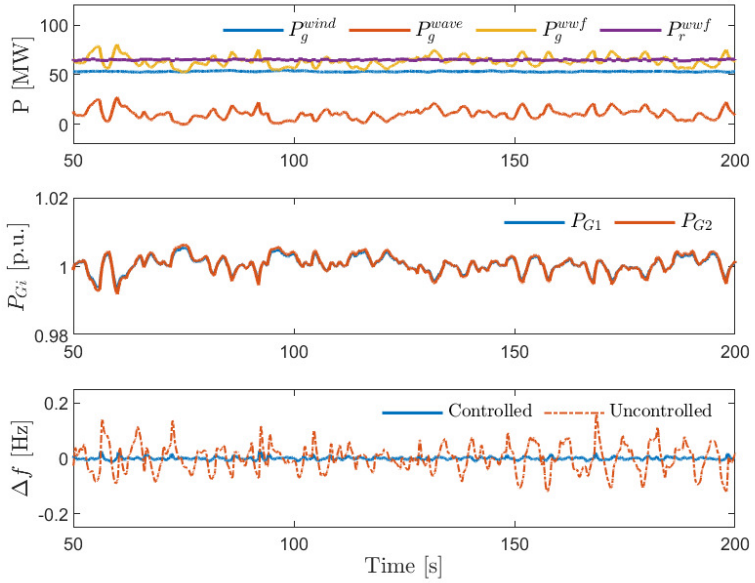

Figure 8: Scenario 2: High wave power absorption

by the onshore generators (P_{G_1},P_{G_2}) decreases during the fault interval in order to compensate the power surplus, as can be seen in the middle plot, verifying the correct operation of the lower-level control. In this way, despite the loss of communications and the consequent power generation failures of the WWF, the low-level control control is capable of ensuring the system stability again, as seen in the bottom plot.

6.4. Scenario 4: Long-Term Operation

The last scenario focuses on the long-term operation of the proposed control scheme. This scenario evaluates the system behavior under wind and wind conditions corresponding to Gran Canaria previously mentioned. These conditions are specified in Table 1 and Table 2. The simulations cover four conditions with a duration of 1 hour:

1. first hour, $H_s = 0.5$, $T_p = 7$ and wind speed between 4 and 6 m/s,
2. second hour, $H_s = 1$, $T_p = 5$ and wind speed between 2 and 4 m/s,
3. third hour, $H_s = 1.5$, $T_p = 6$ and wind speed between 4 and 6 m/s,
4. fourth hour, corresponding to the most demanding conditions, $H_s = 2$, $T_p = 8$ and wind speed between 6 and 8 m/s.

The wind speeds correspond to a height of 10 m, the values faced by the wind turbines are obtained with the expression (37) in the Appendix.

Figure 10 shows the simulation results corresponding to the conditions mentioned above. These results indicate the proposed control strategy works properly also under a diverse wave-wind conditions. Despite the

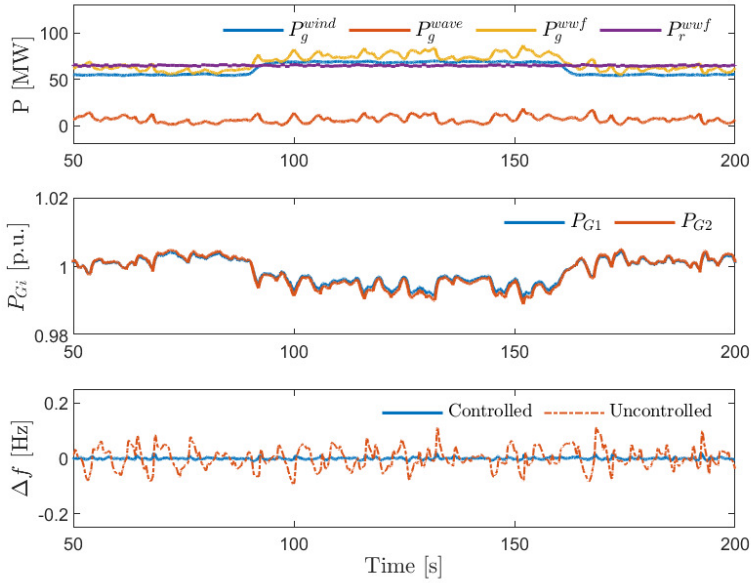

Figure 9: Scenario 3: Communication fault

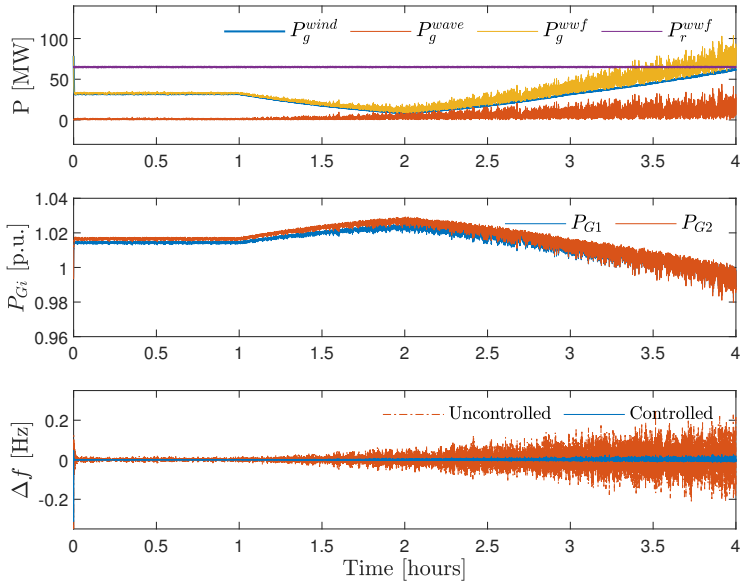

Figure 10: Scenario 4: Long-term simulation corresponding to the most probable conditions on the North-East of Gran Canaria

conditions of Gran Canaria are not as extreme as other offshore implantation areas, the controller is robust in every most probable weather condition. After the second hour, the low wind and wave power conditions forces the onshore generation to increase the power contribution in order to maintain the frequency values. It can be observed that during the lower atmospheric wind-wave states, the fluctuations are lower, due to

State	Max. Δf [Hz]			
	First Hour	Second Hour	Third Hour	Fourth Hour
Uncontrolled	0.04	0.06	0.13	0.22
Controlled	0.0005	0.0009	0.008	0.018

Table 3: Maximum frequency deviations corresponding to the simulations in (Figure 10)

the low generation of the co-located wind-wave farm. As absorption increases, active power fluctuations increase, due to increased wave and wind generation. This means greater frequency fluctuations and greater variability of onshore generators to compensate for deviations. Nevertheless, when the wind and wave power start to increase, the control strategy is able to revert the onshore contributions. Thus, the renewable sources are again generating most of the power demanded by the system. Notice that the frequency regulation is improved under all wind-wave power conditions compared with the uncontrolled case. Table 3 summarizes the maximum frequency deviations under the four wave-wind conditions, confirming the benefits of the proposed scheme.

7. Conclusions

Advances in offshore wind power and wave energy extraction devices are fostering the study of power generation plants combining both sources. Wind and wave power systems can share infrastructure in order to reduce transmission and installation costs. This article presents a complete model for the WWF, including the individual behavior of WEC and wind turbines, and the corresponding power system. It also proposed a two-level control scheme aimed to coordinate both power sources in order to alleviate power generation fluctuations, increase the power reserve of the system whenever possible, and guarantee the system stability. This scheme was evaluated in a realistic case study under nominal and faulty conditions. In all studied scenarios, the proposed control was capable of guarantying a proper frequency regulation. The analysis has also shown that the scheme is also able to increase the power reserve, needed for ancillary services, under high wave energy conditions.

Acknowledgements

The research leading to these results has received financial support from the Research and Universities Department of Catalonia Government under FI2022 program with grant agreement 2022-FI_B-00930.

Appendix

The random sea waves have been approximated by a set of regular wave components with different frequencies and random phases [40, 45]:

	Parameter	Value	Unit
Power	Grid Voltage	230	kV
system	Grid Frequency	50	Hz
	Range of A1 Demand	$100 \pm 10\%$	MW
	Range of A2 Demand	$90 \pm 10\%$	MW
	Range of A3 Demand	$125 \pm 10\%$	MW
	G_1 Rated Power	160	MW
	G_2 Rated Power	75	MW
	Rated Power WWF	90	MW
Wind	Rated Power	5	MW
turbine	Blade Length	61.5	m
	Rated wind speed	11.4	m/s
	Cut-in wind speed	3	m/s
	Cut-out wind speed	25	m/s
	J, T, K and B	see [42]	-
WEC	Mass	360	ton
	Buoy Radius	5	m

Table 4: Parameters corresponding to the study case

$$\begin{aligned} \eta(t) &= \Re\left[\sum_{n=1}^{N} A_n e^{i(\omega_n t+\varepsilon_n)}\right] \\ A_n &= \sqrt{2S\left(\omega_n\right)\omega} \end{aligned} \tag{36}$$

being A_n, ω_n, and ε_n are the amplitude, frequency and random phase of the regular wave component n, respectively. Finally, N corresponds the number of regular wave components in the wave spectrum $S(\omega)$.

On the other hand, due to the wind speed in Table 1 is given at 10 m, the effective wind speed faced by each wind turbine at the hub height can be obtained from:

$$v_{hub} = \left(\frac{h_{hub}}{10}\right)^{1/7} v_{10} \tag{37}$$

where h_{hub} is the height of the turbine hub [46].

References

[1] C. Pérez-Collazo, D. Greaves, G. Iglesias, A review of combined wave and offshore wind energy, Renewable and Sustainable Energy Reviews 42 (2015) 141–153.

[2] S. Astariz, C. Perez-Collazo, J. Abanades, G. Iglesias, Towards the optimal design of a co-located wind-wave farm, Energy 84 (2015) 15–24.

[3] E. D. Stoutenburg, N. Jenkins, M. Z. Jacobson, Power output variations of co-located offshore wind turbines and wave energy converters in california, Renewable Energy 35 (12) (2010) 2781–2791.

[4] M. Veigas, G. Iglesias, Wave and offshore wind potential for the island of Tenerife, Energy Conversion and Management 76 (2013) 738–745.

[5] F. Fusco, G. Nolan, J. V. Ringwood, Variability reduction through optimal combination of wind/wave resources–an irish case study, Energy 35 (1) (2010) 314–325.

[6] S. Astariz, C. Perez-Collazo, J. Abanades, G. Iglesias, Co-located wind-wave farm synergies (operation & maintenance): A case study, Energy Conversion and Management 91 (2015) 63–75.

[7] H. Lund, Large-scale integration of optimal combinations of PV, wind and wave power into the electricity supply, Renewable Energy 31 (4) (2006) 503–515.

[8] E. Stoutenburg, M. Jacobson, Optimizing offshore transmission links for marine renewable energy farms, in: OCEANS 2010 MTS/IEEE SEATTLE, IEEE, 2010, pp. 1–9.

[9] E. Tedeschi, E. Robles, M. Santos, O. Duperray, F. Salcedo, Effect of energy storage on a combined wind and wave energy farm, in: Proceedings of the IEEE Energy Conversion Congress and Exposition (ECCE), IEEE, 2012, pp. 2798–2804.

[10] S. Rasool, K. M. Muttaqi, D. Sutanto, M. Hemer, Quantifying the reduction in power variability of co-located offshore wind-wave farms, Renewable Energy 185 (2022) 1018–1033.

[11] E. Gaughan, B. Fitzgerald, An assessment of the potential for co-located offshore wind and wave farms in Ireland, Energy 200 (2020) 117526.

[12] A. Saenz-Aguirre, J. Saenz, A. Ulazia, G. Ibarra-Berastegui, Optimal strategies of deployment of far offshore co-located wind-wave energy farms, Energy Conversion and Management 251 (2022) 114914.

[13] C. E. Clark, A. Miller, B. DuPont, An analytical cost model for co-located floating wind-wave energy arrays, Renewable Energy 132 (2019) 885–897.

[14] J. Henriques, L. Gato, A. Falcao, E. Robles, F.-X. Faÿ, Latching control of a floating oscillating-water-column wave energy converter, Renewable Energy 90 (2016) 229–241.

[15] A. Babarit, G. Duclos, A. H. Clément, Comparison of latching control strategies for a heaving wave energy device in random sea, Applied Ocean Research 26 (5) (2004) 227–238.

[16] A. Babarit, A. H. Clément, Optimal latching control of a wave energy device in regular and irregular waves, Applied Ocean Research 28 (2) (2006) 77–91.

[17] D. T. Gaebele, M. E. Magaña, T. K. Brekken, J. C. Henriques, A. A. Carrelhas, L. M. Gato, Second order sliding mode control of oscillating water column wave energy converters for power improvement, IEEE Transactions on Sustainable Energy 12 (2) (2020) 1151–1160.

[18] T. Demonte Gonzalez, G. G. Parker, E. Anderlini, W. W. Weaver, Sliding mode control of a nonlinear wave energy converter model, Journal of Marine Science and Engineering 9 (9) (2021) 951.

[19] G. Li, M. R. Belmont, Model predictive control of sea wave energy converters–part i: A convex approach for the case of a single device, Renewable Energy 69 (2014) 453–463.

[20] T. K. Brekken, On model predictive control for a point absorber wave energy converter, in: Proceedings of the IEEE Trondheim PowerTech, IEEE, 2011, pp. 1–8.

[21] G. Bacelli, P. Balitsky, J. V. Ringwood, Coordinated control of arrays of wave energy devices - benefits over independent control, IEEE Transactions on Sustainable Energy 4 (4) (2013) 1091–1099.

[22] F. D. Bianchi, Wind turbine control systems: principles, modelling and gain scheduling design, Vol. 19, Springer.

[23] H. Del Pozo González, J. L. Domínguez-García, Non-centralized hierarchical model predictive control strategy of floating offshore wind farms for fatigue load reduction, Renewable Energy 187 (2022) 248–256.

[24] S. Siniscalchi-Minna, F. D. Bianchi, M. De-Prada-Gil, C. Ocampo-Martinez, A wind farm control strategy for power reserve maximization, Renewable Energy 131 (2019) 37–44.

[25] S. Boersma, B. Doekemeijer, S. Siniscalchi-Minna, J. van Wingerden, A constrained wind farm controller providing secondary frequency regulation: An LES study, Renewable Energy 134 (2019) 639–652.

[26] P. Kundur, Power system stability, Power System Stability and Control 10 (2007).

[27] L. L. Grigsby, Power system stability and control, CRC press, 2007.

[28] R. Ekström, M. Leijon, Control of offshore marine substation for grid-connection of a wave power farm, International Journal of Marine Energy 5 (2014) 24–37.

[29] S. Armstrong, E. Cotilla-Sanchez, T. Kovaltchouk, Assessing the impact of the grid-connected pacific marine energy center wave farm, IEEE Journal of Emerging and Selected Topics in Power Electronics 3 (4) (2015) 1011–1020.

[30] I. M. Sanz, B. Chaudhuri, G. Strbac, Inertial response from offshore wind farms connected through DC grids, IEEE Transactions on Power Systems 30 (3) (2014) 1518–1527.

[31] F. D. Bianchi, J. L. Dominguez-Garcia, Coordinated frequency control using MT-HVDC grids with wind power plants, IEEE Transactions on Sustainable Energy 7 (1) (2016) 213–220.

[32] F. D. Bianchi, J. L. Domínguez-García, T. K. Vrana, Distributed frequency control with partial information using MT-HVDC grids and WPPs, IEEE Systems Journal 13 (2) (2018) 1694–1701.

[33] F. Vigara, L. Cerdán, R. Durán, S. Muñoz, M. Lynch, S. Doole, C. Molins, P. Trubat, R. Gunache, Design basis (Sep. 2020). doi:10.5281/zenodo.4518828.

[34] O. Faltinsen, Sea loads on ships and offshore structures, Vol. 1, Cambridge University Press, 1993.

[35] J. Falnes, Wave-energy conversion through relative motion between two single-mode oscillating bodies, Journal of Offshore Mechanics and Arctic Engineering 121 (1) (1999) 32–38.

[36] J. J. Cândido, P. A. Justino, Modelling, control and Pontryagin maximum principle for a two-body wave energy device, Renewable Energy 36 (5) (2011) 1545–1557.

[37] A. F. Falcão, J. C. Henriques, J. J. Cândido, Dynamics and optimization of the OWC spar buoy wave energy converter, Renewable Energy 48 (2012) 369–381.

[38] R. Gomes, J. Henriques, L. Gato, A. Falcão, Time-domain simulation of a slack-moored floating oscillating water column and validation with physical model tests, Renewable Energy 149 (2020) 165–180.

[39] K. Budal, J. Falnes, Optimum operation of improved wave-power converter, Mar. Sci. Commun.;(United States) 3 (2) (1977).

[40] J. Falnes, A. Kurniawan, Ocean waves and oscillating systems: linear interactions including wave-energy extraction, Vol. 8, Cambridge University Press, 2020.

[41] W. Cummins, W. Iiuhl, A. Uinm, The impulse response function and ship motions (1962).

[42] J. Jonkman, S. Butterfield, W. Musial, G. Scott, Definition of a 5-MW reference wind turbine for offshore system development, Tech. rep., National Renewable Energy Lab.(NREL), Golden, CO (United States) (2009).

[43] P. Sørensen, A. D. Hansen, F. Iov, F. Blaabjerg, M. H. Donovan, Wind farm models and control strategies (Aug 2005).

[44] Y.-n. Yu, K. Vongsuriya, L. N. Wedman, Application of an optimal control theory to a power system, IEEE Transactions on Power Apparatus and Systems (1) (1970) 55–62.

[45] L. Li, Z. Yuan, Y. Gao, Maximization of energy absorption for a wave energy converter using the deep machine learning, Energy 165 (2018) 340–349.

[46] T. Burton, N. Jenkins, D. Sharpe, E. Bossanyi, Wind energy handbook, John Wiley & Sons, 2011.